Supporting Information

A cyanide-bridged wheel featuring a seven-coordinate Mo(III) center

David K. Kempe, Brian S. Dolinar, Kuduva R. Vignesh, Toby J. Woods, Mohamed R. Saber, and Kim R. Dunbar*

Table of Contents

Synthetic Details 2
Table S1. Crystal data and structure refinement for Mo^{III} wheel 4
Table S2. Crystal data and structure refinement for Mo^{IV} wheel 5
Table S3. Comparison of the unit cells of Mo^{III} and Mo^{IV} wheels 6
Table S4. SHAPE results for Mo centers in Mo^{III} wheel 6
Figure S1. Asymmetric unit of Mo^{III} wheel 7
Figure S2. Local geometry of the molybdenum atoms in Mo^{III} wheel 7
Table S5. Selected bond distances (Å) for Mo^{III} wheel 8
Table S6. Selected bond angles (°) for Mo^{III} wheel 9
Infrared Spectroscopy Details 11
Figure S3. IR spectra 12
SQUID Magnetometry Details 13
Figure S4. Reduced magnetization data 13
Computational Details 13
Figure S5. Fragment used for DFT calcuations 14
Table S7. Spin configurations for metal atoms 14
Figure S6. Fragments used for *ab initio* calculations 16
Table S8. g, *D,* and *E/D* values for both Ni centers 17
Table S9. Contributions to *D* from excited states 17
References 17

Synthetic Details

Syntheses were carried out under air free conditions using a nitrogen-filled glove box or Schlenk line outfitted with argon gas. The solvents were deoxygenated by sparging with argon gas. $Mo^{III}Cl_3(THF)_3$ and $Ni(L)(ClO_4)_2$ were prepared by literature methods[1,2]; all other chemicals were purchased from commercial sources and used without further purification unless otherwise indicated.

Synthesis of $K_4[Mo(CN)_7]\cdot 2H_2O$

A 3.2g (7.64 mmol) sample of $Mo^{III}Cl_3(THF)_3$ and 4.4g (66.9 mmol) of KCN were added to a flask containing 40 mL of water and heated to 70°C for 12 h to yield a dark orange solution. Methanol was subsequently added until the solution became slightly cloudy. After left to stand overnight at -25˚C, X-ray quality dark olive green crystals were isolated (2.48g, 69% yield).

Synthesis of $[Mo^{III}(CN)_7]_6[Ni(L)]_{12}\cdot 24H_2O$ ($Mo^{III}_6Ni_{12}$)

A 25mg (0.05 mmol) sample of $K_4[Mo^{III}(CN)_7]\cdot 2H_2O$ was dissolved in 6 mL of water. A separate sample (25mg, 0.05 mmol) of Ni(L) was dissolved in 6 mL of water and added dropwise to the solution of $K_4[Mo^{III}(CN)_7]\cdot 2H_2O$. After standing overnight, the dark orange needle crystals were collected by filtration and washed with H_2O and Et_2O, 27mg, 50% yield. Samples were dried under vacuum prior to submission for elemental analysis and SQUID measurements. Found: C, 44.94; N, 21.34; H, 5.17%. Calc. for $[Mo^{III}(CN)_7]_6[Ni(L)]_{12}\cdot 24H_2O$: C, 45.15; N, 21.35; H, 5.33%.

Synthesis of $[Mo^{IV}(CN)_8]_6[Ni(L)]_{12}\cdot 30H_2O$ ($Mo^{IV}_6Ni_{12}$)

A 65 mg sample of $K_4[Mo(CN)_8]\cdot 2H_2O$ was dissolved in 8 mL of water. A separate 50 mg sample of Ni(L) was dissolved in 8 mL of water and added dropwise to the solution of $K_4[Mo(CN)_8]\cdot 2H_2O$. After standing overnight, dark yellow needle crystals were collected by filtration and washed with H_2O and Et_2O, 34 mg, 32% yield. The sample was dried under vacuum prior to submission for elemental analysis and SQUID measurements.

Found: C, 44.40; N, 21.74; H, 5.22%. Calc for $[Mo^{IV}(CN)_8]_6[Ni(L)]_{12}\cdot 30H_2O$: C, 44.39; N, 21.79; H, 5.29%.

Crystallographic Details

$Mo_6^{III}Ni_{12}$

Single crystals of $Mo_6^{III}Ni_{12}$ were selected under ®Paratone oil with a MiTeGen microloop. Reflection data were collected on a Bruker D8-QUEST diffractometer equipped with a IμS Mo microsource (λ = 0.71073 Å) and under a stream of N_2 gas a 110 K. The frames were integrated and a semi-empirical absorption correction was applied using SADABS[3] within the software package included in the APEX3 software suite.[4] The structure was solved using SHELXT[5] and refined using SHELXL;[6] OLEX2 was used as an interface for the solution and refinement.[7] Small Q-peaks in the structure that were consistent with the behavior of disordered solvent were removed using the SQUEEZE routine of the PLATON software package.[8] Hydrogen atoms were placed in calculated positions.

Three of the CN^- ligands in the structure are disordered (one of the axial ligands on each Mo center). The CN^- ligand on Mo1 is disordered in a 0.644:0.356(16) ratio, on Mo2 in a 0.730:0.230(15) ratio, and on Mo3 in a 0.55:0.45(2) ratio. There is also disorder in the ligand on the terminal Ni centers that corresponds to an in-plane twist. For Ni2, the ligand is disordered in a ratio of 0.617:0.383(6), and for Ni6 the ligand is disordered in a ratio of 0.543:0.457(6). Ni4 itself is disordered along with the ligand in a ratio of 0.904:0.096(5).

$Mo_6^{IV}Ni_{12}$

Single crystals of $Mo_6^{IV}Ni_{12}$ were selected under ®Paratone oil with a MiTeGen microloop. Reflection data were collected on a Bruker D8-Venture diffractometer equipped with a IμS Cu microsource (λ = 1.54178) and under a stream of N_2 gas at 110 K. The frames were integrated and a semi-empirical absorption correction was applied using SADABS[3] within the software package included in the APEX3 software suite.[4] The structure was solved using SHELXT[5] and refined using SHELXL;[6] OLEX2 was used as an interface for the solution and refinement.[7] Small Q-peaks in the structure that were consistent with the behavior of disordered solvent were accounted for with a solvent mask within OLEX2. Hydrogen atoms were placed in calculated positions.

Table S1. Crystal data and structure refinement for $\mathbf{Mo_6^{III}Ni_{12}}$

Identification code	$\mathbf{Mo_6^{III}Ni_{12}}$
Empirical formula	$C_{222}H_{276}Mo_6N_{90}Ni_{12}O_6$
Formula weight	5581.47
Temperature/K	110.0
Crystal system	triclinic
Space group	$P\bar{1}$
a/Å	20.8632(17)
b/Å	20.9777(19)
c/Å	21.0033(18)
α/°	105.168(3)
β/°	105.407(2)
γ/°	104.914(2)
Volume (Å^3)	8008.0(12)
Z	1
ρ_{calc}g (cm^3)	1.157
μ (mm^{-1})	0.968
F (000)	2874.0
Crystal size (mm^3)	0.5 × 0.2 × 0.05
Radiation	MoKα (λ = 0.71073)
2Θ range for data collection/°	4.068 to 48.602
Index ranges	-24 ≤ h ≤ 24, -24 ≤ k ≤ 24, -24 ≤ l ≤ 24
Reflections collected	89054
Independent reflections	25768 [R_{int} = 0.0848, R_{sigma} = 0.0814]
Data/restraints/parameters	25768/2764/2122
Goodness-of-fit[a] on F^2	1.030
Final R indexes [I>=2σ (I)]	R_1[b] = 0.0881, wR_2[c] = 0.1838
Final R indexes [all data]	R_1[b] = 0.1361, wR_2[c] = 0.2110
Largest diff. peak/hole / e Å^{-3}	0.96/-1.01

[a]Goodness-of-fit = $\{\Sigma [w(Fo^2 - Fc^2)^2]/(n-p)\}^{1/2}$, where n is the number of reflections and p is the total number of parameters refined.

[b]$R = \Sigma \| Fo | - | Fc \| / \Sigma | Fo |$

[c]$wR = \{\Sigma [w(Fo^2 - Fc^2)^2] / \Sigma w(Fo^2)^2]\}^{1/2}$

Table S2. Crystal data and structure refinement for $\mathbf{Mo_6^{IV}Ni_{12}}$

Identification code	$\mathbf{Mo_6^{IV}Ni_{12}}$
Empirical formula	$C_{38}H_{46}MoN_{16}Ni_2O$
Formula weight	956.27
Temperature/K	100.0
Crystal system	trigonal
Space group	$R\bar{3}$
a/Å	33.6548(8)
b/Å	33.6548(8)
c/Å	24.8190(6)
α/°	90
β/°	90
γ/°	120
Volume/Å^3	24344.9(13)
Z	18
ρ_{calc}g (cm^3)	1.174
μ (mm^{-1})	3.005
F(000)	8856.0
Crystal size (mm^3)	0.8 × 0.2 × 0.2
Radiation	CuKα (λ = 1.54178)
2Θ range for data collection (°)	7.034 to 140.406
Index ranges	-41 ≤ h ≤ 41, -41 ≤ k ≤ 35, -30 ≤ l ≤ 30
Reflections collected	84785
Independent reflections	10294 [R_{int} = 0.0522, R_{sigma} = 0.0260]
Data/restraints/parameters	10294/1/543
Goodness-of-fit[a] on F^2	1.051
Final R indexes [I>=2σ (I)]	R_1 = 0.0346, wR_2 = 0.0863
Final R indexes [all data]	R_1 = 0.0418, wR_2 = 0.0894
Largest diff. peak/hole / e Å^{-3}	0.67/-0.43

[a]Goodness-of-fit = $\{\Sigma [w(Fo^2 - Fc^2)^2]/(n-p)\}^{1/2}$, where n is the number of reflections and p is the total number of parameters refined.

[b]$R = \Sigma \| Fo | - | Fc \| / \Sigma | Fo |$

[c]$wR = \{\Sigma [w(Fo^2 - Fc^2)^2] / \Sigma w(Fo^2)^2]\}^{1/2}$

Table S3. Comparison of the unit cell parameters for $\mathbf{Mo_6^{IV}Ni_{12}}$ and $\mathbf{Mo_6^{III}Ni_{12}}$.

Unit cell parameter	$\mathbf{Mo_6^{IV}Ni_{12}}$	$\mathbf{Mo_6^{III}Ni_{12}}$
Space Group	$R\bar{3}$	$P\bar{1}$
a (Å)	21.1191(3)	20.8632(17)
b (Å)	21.1191(3)	20.9777(19)
c (Å)	21.1191(3)	21.0033(18)
α (°)	105.6515(6)	105.168(3)
β (°)	105.6515(6)	105.407(2)
γ (°)	105.6515(6)	104.914(2)
V (Å^3)	8116.0(2)	8008.1(12)

Table S4. SHAPE results for crystallographically independent Mo^{III} centers in $\mathbf{Mo_6^{III}Ni_{12}}$.

Mo Center	CShM for Pentagonal Bipyramidal	CShM value for Capped Trigonal Prism
1	2.530	2.316
2	2.441	2.233
3	3.849	0.924

Figure S1. Asymmetric unit of $\mathbf{Mo_6^{III}Ni_{12}}$

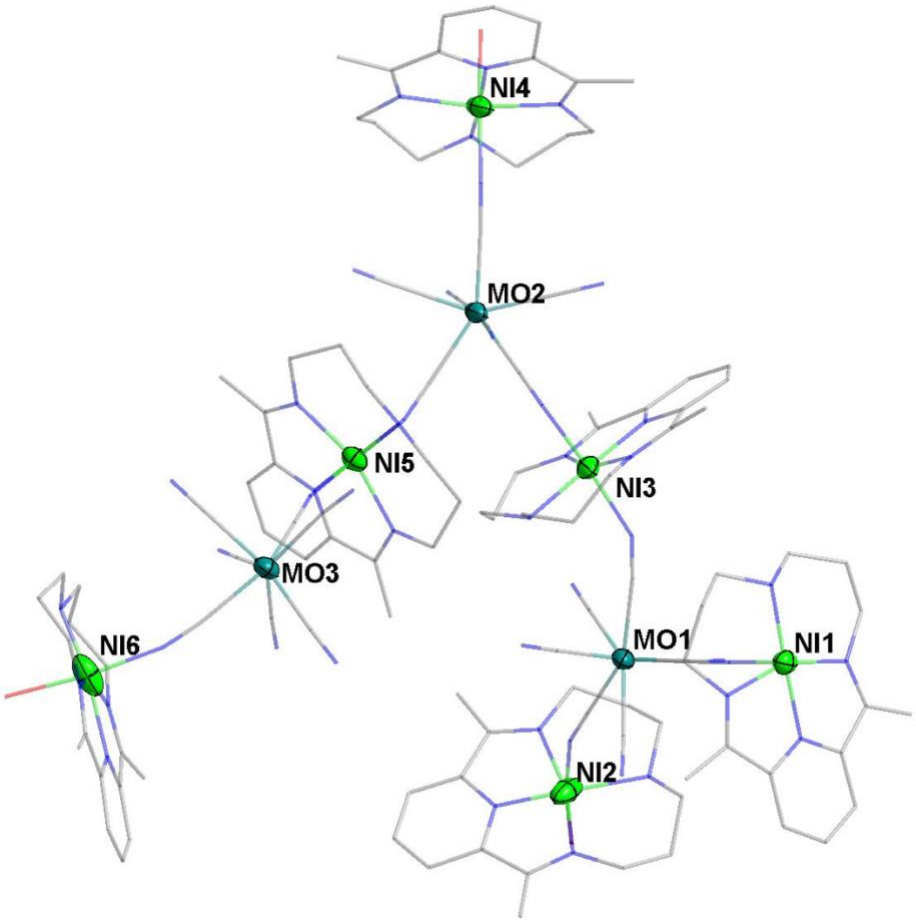

Figure S2. Local geometry of the molybdenum atoms in $\mathbf{Mo_6^{III}Ni_{12}}$ (Mo1, Mo2, and Mo3 left to right)

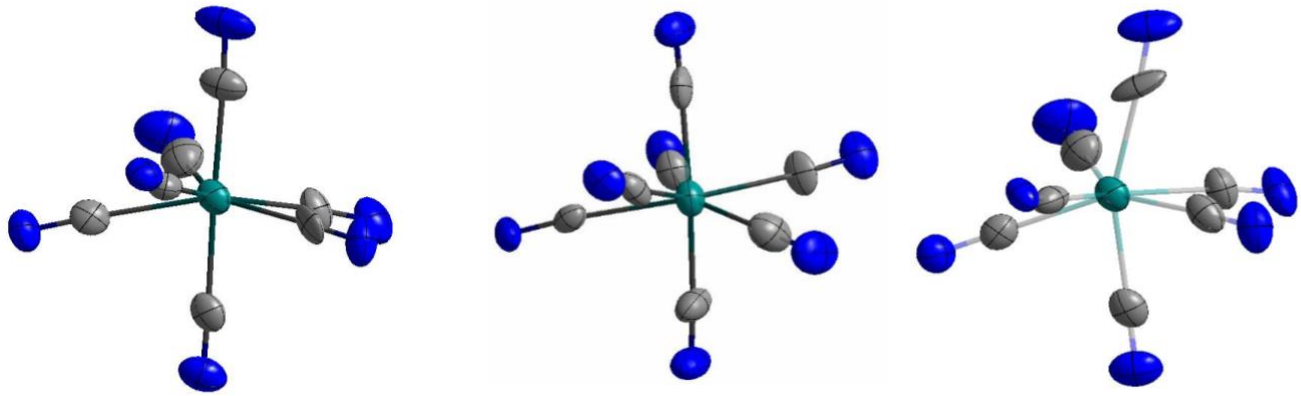

Table S5. Selected bond distances (Å) for $\mathbf{Mo_6^{III}Ni_{12}}$

Mo1	C91	2.141(10)
Mo1	C92	2.146(10)
Mo1	C93	2.141(10)
Mo1	C94	2.152(13)
Mo1	C95	2.169(10)
Mo1	C96	2.178(11)
Mo1	C97	2.143(14)
Mo1	C97A	2.24(2)
Mo2	C98	2.135(10)
Mo2	C99	2.119(9)
Mo2	C100	2.163(9)
Mo2	C101	2.170(9)
Mo2	C102	2.118(15)
Mo2	C103	2.130(11)
Mo2	C104	2.170(11)
Mo2	C1B	2.37(5)
Mo3	C105	2.100(10)
Mo3	C106	2.159(10)
Mo3	C107	2.172(11)
Mo3	C108	2.175(11)
Mo3	C109	2.189(11)
Mo3	C110	2.140(11)
Mo3	C111	2.149(18)
Mo3	C1A	2.17(2)
Ni1	N27	2.066(8)
Ni1	N41	2.108(8)
Ni1	N1	1.974(6)
Ni1	N2	2.057(6)
Ni1	N3	2.009(6)
Ni1	N4	2.064(6)
Ni2	O1	2.194(8)
Ni2	N25	2.036(9)
Ni2	N5	1.833(7)
Ni2	N6	2.113(8)
Ni2	N7	2.156(8)
Ni2	N8	1.955(8)
Ni2	N5A	2.220(10)
Ni2	N6A	2.055(10)

Ni2	N7A	1.766(11)
Ni2	N8A	2.187(11)
Ni3	N9	1.964(8)
Ni3	N10	2.065(8)
Ni3	N11	2.042(8)
Ni3	N12	2.041(9)
Ni3	N26	2.116(8)
Ni3	N32	2.060(8)
Ni4	O2	2.186(8)
Ni4	N33	2.069(9)
Ni4	N13	1.917(7)
Ni4	N14	2.077(7)
Ni4	N15	2.052(7)
Ni4	N16	2.026(7)
Ni5	N17	1.956(7)
Ni5	N20	2.049(8)
Ni5	N19	2.033(8)
Ni5	N18	2.066(8)
Ni5	N34	2.110(8)
Ni5	N39	2.071(8)
Ni6	O3	2.174(8)
Ni6	N40	2.049(9)
Ni6	N21	2.134(8)
Ni6	N22	2.125(8)
Ni6	N23	1.844(8)
Ni6	N24	2.069(8)
Ni6	N21A	1.735(9)
Ni6	N22A	1.912(10)
Ni6	N23A	2.247(9)
Ni6	N24A	2.141(9)

Table S6. Selected bond angles (˚) for $\mathbf{Mo_6^{III}Ni_{12}}$

C91	Mo1	C92	148.6(3)
C91	Mo1	C94	73.1(4)
C91	Mo1	C95	83.5(3)
C91	Mo1	C96	75.0(3)
C91	Mo1	C97	97.8(6)
C91	Mo1	C97A	79.2(9)
C92	Mo1	C94	135.0(4)
C92	Mo1	C95	98.2(3)
C92	Mo1	C96	74.3(3)

C92	Mo1	C97A	87.8(8)
C93	Mo1	C91	134.2(3)
C93	Mo1	C92	75.8(3)
C93	Mo1	C94	73.1(4)
C93	Mo1	C95	76.6(3)
C93	Mo1	C96	139.3(3)
C93	Mo1	C97	105.6(6)
C93	Mo1	C97A	127.8(9)
C94	Mo1	C95	105.1(4)
C94	Mo1	C96	146.4(4)
C94	Mo1	C97A	86.4(8)
C95	Mo1	C96	81.1(3)
C95	Mo1	C97A	155.5(10)
C96	Mo1	C97A	77.8(9)
C97	Mo1	C92	78.1(5)
C97	Mo1	C94	79.8(5)
C97	Mo1	C95	175.0(5)
C97	Mo1	C96	94.6(6)
C98	Mo2	C100	75.6(3)
C98	Mo2	C101	139.9(4)
C98	Mo2	C104	77.2(3)
C98	Mo2	C1B	129.8(13)
C99	Mo2	C98	134.7(3)
C99	Mo2	C100	148.1(3)
C99	Mo2	C101	74.5(3)
C99	Mo2	C103	74.1(4)
C99	Mo2	C104	83.1(4)
C99	Mo2	C1B	78.5(12)
C100	Mo2	C101	74.1(3)
C100	Mo2	C104	97.7(3)
C100	Mo2	C1B	87.8(10)
C101	Mo2	C1B	74.3(11)
C102	Mo2	C98	105.5(6)
C102	Mo2	C99	97.6(5)
C102	Mo2	C100	79.1(4)
C102	Mo2	C101	93.8(5)
C102	Mo2	C103	79.4(5)
C102	Mo2	C104	175.0(5)
C103	Mo2	C98	72.7(4)
C103	Mo2	C100	134.8(4)
C103	Mo2	C101	146.6(4)
C103	Mo2	C104	105.5(4)

C103	Mo2	C1B	88.5(10)
C104	Mo2	C101	81.6(3)
C104	Mo2	C1B	152.8(12)
C105	Mo3	C106	131.1(3)
C105	Mo3	C107	76.4(3)
C105	Mo3	C108	75.5(3)
C105	Mo3	C109	139.5(3)
C105	Mo3	C110	71.9(4)
C105	Mo3	C111	124.7(8)
C105	Mo3	C1A	103.9(10)
C106	Mo3	C107	150.5(3)
C106	Mo3	C108	82.9(4)
C106	Mo3	C109	75.9(3)
C106	Mo3	C1A	101.8(10)
C107	Mo3	C108	96.8(3)
C107	Mo3	C109	75.0(3)
C108	Mo3	C109	80.1(4)
C110	Mo3	C106	73.8(4)
C110	Mo3	C107	133.0(4)
C110	Mo3	C108	107.4(4)
C110	Mo3	C109	147.4(4)
C110	Mo3	C111	84.5(7)
C110	Mo3	C1A	78.2(8)
C111	Mo3	C106	84.6(7)
C111	Mo3	C107	86.2(6)
C111	Mo3	C108	159.5(8)
C111	Mo3	C109	81.1(7)
C1A	Mo3	C107	76.9(8)
C1A	Mo3	C108	173.6(8)
C1A	Mo3	C109	96.8(9)

Infrared Spectroscopy Details

Infrared spectra were collected on a Nicolet 740 Fourier transform IR spectrometer.

Samples were prepared and measured as a ®Nujol mulls between KBr plates.

Figure S3. IR spectra for $\mathbf{Mo_6^{III}Ni_{12}}$ and $\mathbf{Mo_6^{IV}Ni_{12}}$. a) Spectra from 4000-400 cm^{-1}. Large peaks at 2900, 1460, and 1377 are from the Nujol used in the mull. b) Spectra from the region that contains the cyanide stretching frequencies (2200-2000 cm^{-1})

a)

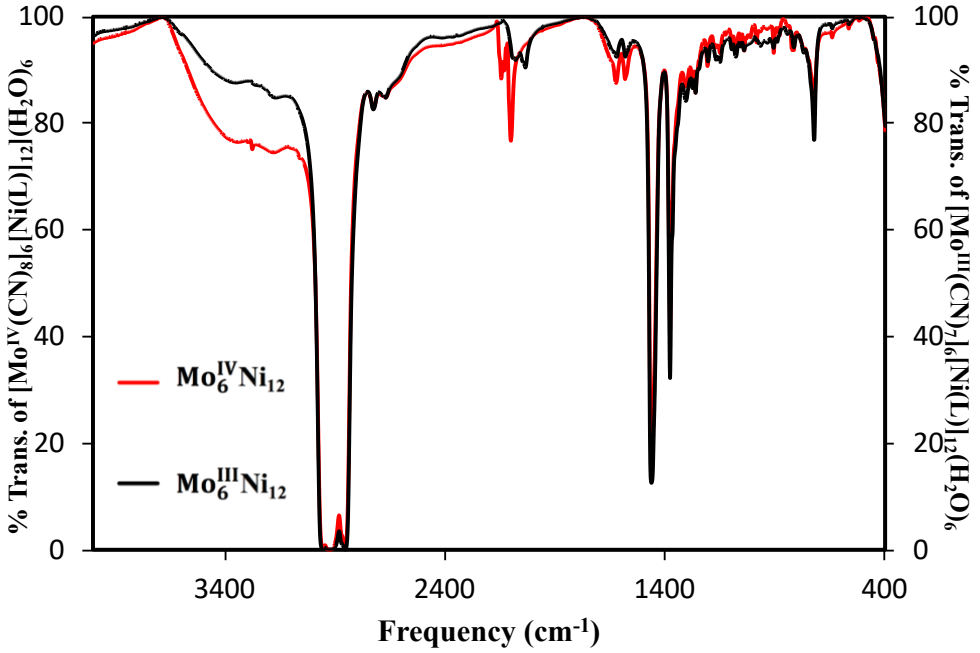

b)

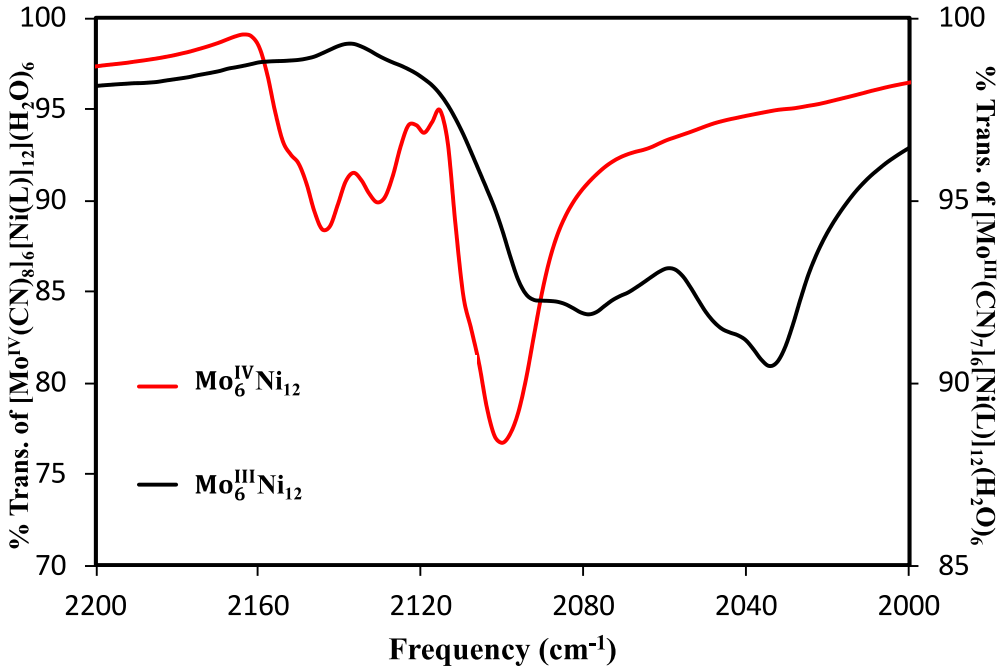

SQUID Magnetometry Details

Measurements were performed on a Quantum Design MPMS-XL SQUID magnetometer equipped with a 7 T magnet. A polypropylene bag was used to secure the sample, and the diamagnetic contribution was subtracted from the raw data. Diamagnetic contributions from the sample were accounted for by using Pascal's constants.[9]

Figure S4. Reduced magnetization of $\mathbf{Mo_6^{III}Ni_{12}}$. Solid lines are a guide for the eye.

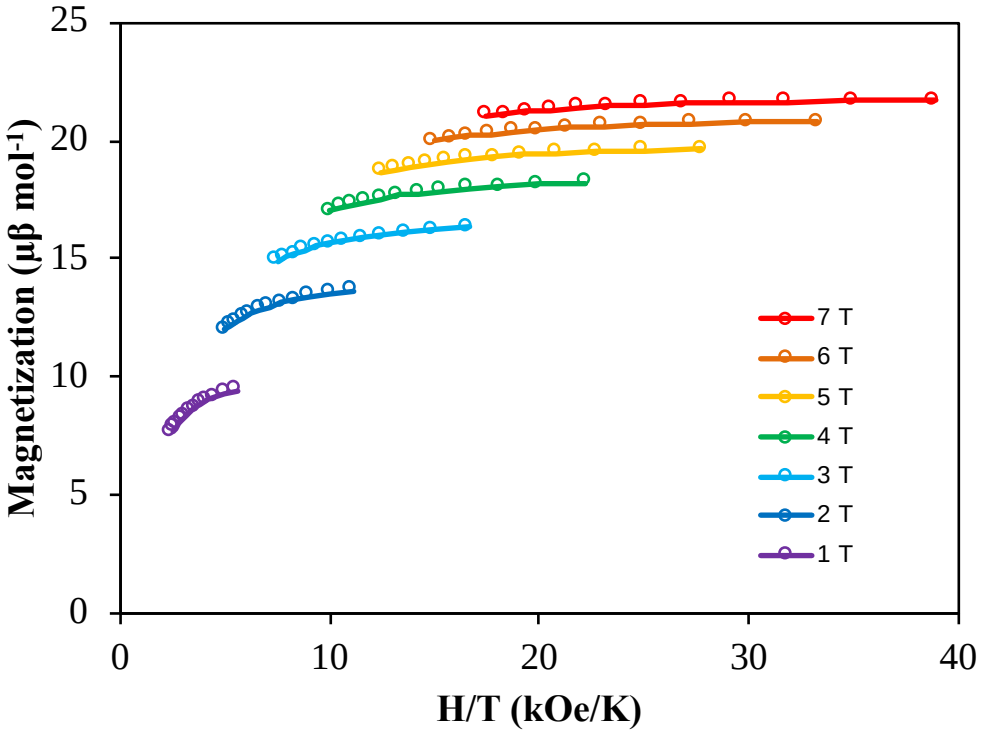

Computational Details

DFT calculations, combinated with the Broken-Symmetry (BS) approach have been employed to compute the exchange interactions. We employed B3LYP[10] functionals with Ahlrichs[11,12] triple-ζ basis set for Ni atoms, a relativistic effective-core potential (ECP) LANL08(f) basis set [13] for Mo atoms and 6-31g* basis set for rest of the atoms as implemented in the Gaussian 09[14] suite of programs to calculate the energies of the spin states as given in Table S5. The *J* values were computed from the energy differences between the high spin (E_{HS}) state calculated using single determinant wave functions, and the low spin (E_{BS}) state determined using the Broken Symmetry (BS)

approach developed by Noodleman.[15] The BS approach has a proven record of yielding good numerical estimates of *J* constants for a variety of complexes,[16,17] such as dinuclear[18-20], and especially, 4d/5d metal complexes[21] and polynuclear complexes.[16,22,23] The following Hamiltonian is used to estimate the isotropic exchange interaction (*J*).

$$\hat{\mathrm{H}} = -2J(S_{\mathrm{Mo}}S_{\mathrm{Ni}})$$

Figure S5. One half of the $\mathbf{Mo_6^{III}Ni_{12}}$ complex, shown below, was used for DFT calculations to compute the exchange interactions

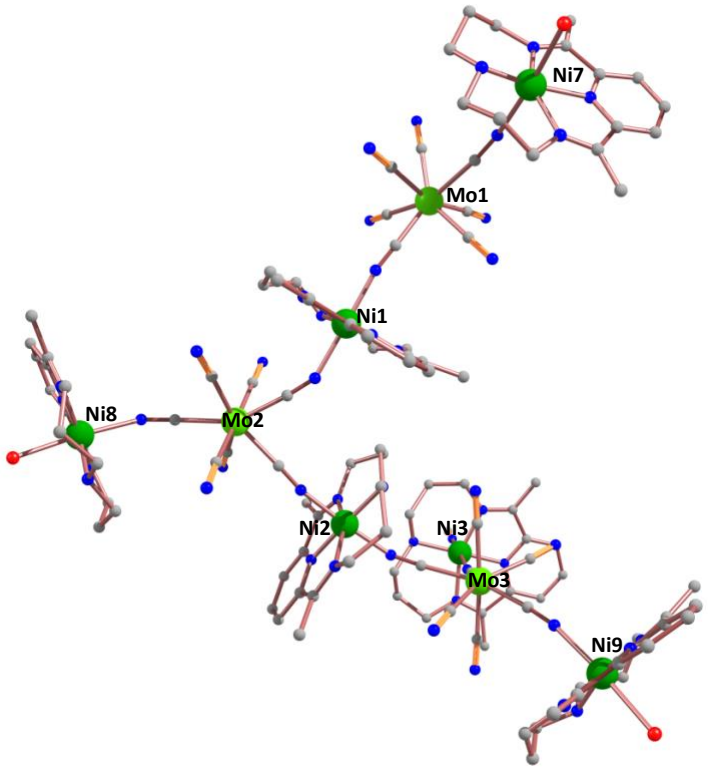

Table S7. Different spin configurations employed for extracting *J* values and its corresponding energies from DFT calcualtions in $\mathbf{Mo_6^{III}Ni_{12}}$

	Mo1	**Mo2**	**Mo3**	**Ni1**	**Ni2**	**Ni3**	**Ni7**	**Ni8**	**Ni9**	**Es (in Hartree)**	$\Delta E = E_{BS} - E_{HS}$ (cm^{-1})
HS	↑	↑	↑	↑	↑	↑	↑	↑	↑	-16346.72018710	0
BS1	↑	↑	↑	↓	↓	↓	↑	↑	↑	-16346.71934660	184.47
BS2	↑	↑	↑	↑	↑	↑	↓	↓	↓	-16346.71984830	74.36

In the case of a two spin system and using the spin Hamiltonian $\mathbf{H = -2J_{ij}S_iS_j}$, the energy difference between the high spin and low spin state is:

$E_{HS} - E_{BS}/2S_iS_j = -2J_{ij}$

Considerations related to the self-interaction error in commonly used exchange functional, non-dynamic pair correlation effects, and the application of spin projection techniques to DFT calculations led to the following equation to describe the energy difference: [16,17,18-20]

$E_{HS} - E_{BS}/(2S_iS_j + S_j) = -2J_{ij}$, where $S_i > S_j$.

Application of this formalism to half of the $Mo^{III}_6Ni^{II}_{12}$ complex that consists of six Ni^{II} ions and three Mo^{III} with three J_1 interactions (between the inner ring Ni^{II} ions and Mo^{III} ions) and three J_2 interactions (between the outer Ni^{II} ions and Mo^{III} ions), leads to the following expressions for the differences between the energies for the nine spin states calculated by DFT methods:

$$E_{BS1} - E_{HS} = 2J_1\left(2 * 1 * \frac{1}{2} + \frac{1}{2}\right) = 3J_1$$

For three possible J_1 interactions the expression becomes, $E_{\mathrm{BS1}} - E_{\mathrm{HS}} = 9J_1$

Similarly, for three possible J_2 interactions the expression becomes, $E_{BS2} - E_{HS} = 9J_2$

$$J_1 = \frac{1}{9}(184.47\ cm^{-1}) = +20.5\ cm^{-1}$$
$$J_2 = \frac{1}{9}\ (74.36\ cm^{-1}) = +8.26\ cm^{-1}$$

We have performed *ab initio* calculations to compute the *g* value and the zero field splitting (D) of the Ni^{II} ions and g value for the Mo^{III} ions in **1** using ORCA 3.0 suite of programs.[24] We employed the BP86 functional along with a scalar relativistic ZORA Hamiltonian and relativistic ZORA type of def2-TZVP basis set on the metal ions and on first coordination sphere, and def2-SVP for the rest of the atoms. The RI approximation with secondary TZV/*J* Columbic fitting basis sets were used along with increased integration grids (Grid 5 in ORCA convention). The tight SCF convergence was used throughout the calculations ($1x10^{-8}$ Eh). The SOC contributions in the *ab initio* frame work were obtained using second-order perturbation theory as well as employing the effective Hamiltonian approach which enables calculations of all matrix elements to be made of the anisotropic spin Hamiltonian from the *ab initio* energies and wave functions numerically. Here we have

employed the state average-CASSCF (Complete Active Space Self-Consistent Field) method to compute the ZFS. The active space comprises eight active electrons in five active d-orbitals (d^8 system; CAS (8,5)) for Ni^{II} ion. With this active space, we computed all 10 triplet and 15 singlet states for the Ni^{II} ion in the configuration interaction procedure.

Figure S6. CASSCF-computed d-orbital ordering for Mo^{III} ions in $\mathbf{Mo_6^{III}Ni_{12}}$.

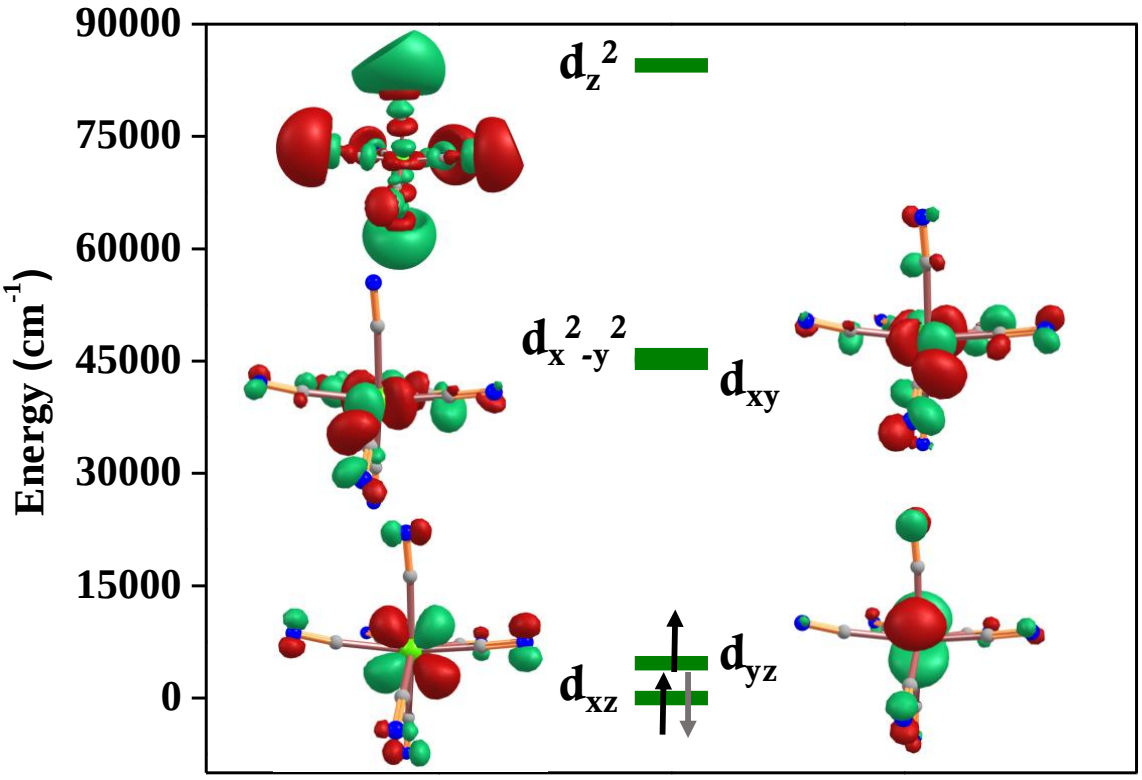

Figure S7. The two Ni centers {$Ni(CN)_2$} (left) and {$Ni(CN)(H_2O)$} (right) used for CASSCF calculations

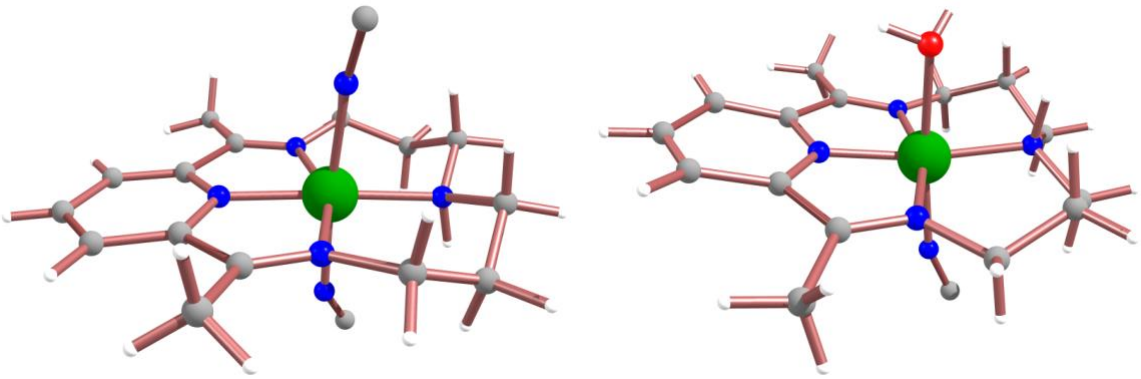

Table S8. g, *D* (in cm^{-1}) and *E/D* values for both Ni and Mo centers in $\mathbf{Mo_6^{III}Ni_{12}}$ computed from *ab initio* CASSCF calculations

Complex	*calculated*		
	D	*E/D*	g_{iso} (g_x, g_y and g_z)
{Ni(CN)$_2$}	-6.2	0.13	2.23 (2.21, 2.22, 2.26)
{Ni(CN)(H$_2$O)}	+11.2	0.23	2.24 (2.18, 2.25, 2.29)
{Mo(CN)$_7$}	--	--	1.76 (1.03, 1.05, 3.19)

Table S9. CASSCF computed energies (cm^{-1}) and contributions to the *D* value from first four excited states for Ni^{II} ions in complex $\mathbf{Mo_6^{III}Ni_{12}}$

Ni centers	Excited state	Energy	*D* Contribution
{Ni(CN)$_2$}	First	8751.7	-48.3
	Second	10199.1	20.7
	Third	10556.6	19.6
	Fourth	16398.0	0.06
{Ni(CN)(H$_2$O)}	First	7830.4	26.7
	Second	8748.8	23.3
	Third	11663.6	-35.6
	Fourth	15349.5	-0.5

References

1 S. Maria, R. Poli, K. J. Gallagher, A. S. Hock and M. J. A. Johnson, in *Inorganic Syntheses: Volume 36*, John Wiley & Sons, Inc., 2014, DOI: 10.1002/9781118744994.ch03, pp. 15-18.

2 J. L. Karn and D. H. Busch, *Inorg. Chem.*, 1969, **8**, 1149-1153.

3 L. Krause, R. Herbst-Irmer, G. M. Sheldrick and D. Stalke, *Journal of Applied Crystallography*, 2015, **48**, 3-10.

4 APEX3 (1), Bruker AXS Inc., Madison, WI, 2016.

5 G. Sheldrick, *Acta Crystallographica Section A*, 2015, **71**, 3-8.

6 G. Sheldrick, *Acta. Cryst.*, 2015, **71**, 3-8.

7 O. V. Dolomanov, L. J. Bourhis, R. J. Gildea, J. A. K. Howard and H. Puschmann, *Journal of Applied Crystallography*, 2009, **42**, 339-341.
8 A. Spek, *Journal of Applied Crystallography*, 2003, **36**, 7-13.
9 G. A. Bain and J. F. Berry, *J. Chem. Ed.*, 2008, **85**, 532.
10 A. D. Becke, *Journal of Chemical Physics*, 1993, **98**, 5648-5652.
11 A. Schaefer, H. Horn and R. Ahlrichs, *Journal of Chemical Physics*, 1992, **97**, 2571-2577.
12 A. Schaefer, C. Huber and R. Ahlrichs, *Journal of Chemical Physics*, 1994, **100**, 5829-5835.
13 P. J. Hay and W. R. Wadt, *The Journal of Chemical Physics*, 1985, **82**, 270-283.
14 M. J. Frisch, G. W. Trucks, H. B. Schlegel, G. E. Scuseria, M. A. Robb, J. R. Cheeseman, G. Scalmani, V. Barone, B. Mennucci, G. A. Petersson, H. Nakatsuji, M. Caricato, X. Li, H. P. Hratchian, A. F. Izmaylov, J. Bloino, G. Zheng, J. L. Sonnenberg, M. Hada, M. Ehara, K. Toyota, R. Fukuda, J. Hasegawa, M. Ishida, T. Nakajima, Y. Honda, O. Kitao, H. Nakai, T. Vreven, J. A. Montgomery Jr., J. E. Peralta, F. Ogliaro, M. J. Bearpark, J. Heyd, E. N. Brothers, K. N. Kudin, V. N. Staroverov, R. Kobayashi, J. Normand, K. Raghavachari, A. P. Rendell, J. C. Burant, S. S. Iyengar, J. Tomasi, M. Cossi, N. Rega, N. J. Millam, M. Klene, J. E. Knox, J. B. Cross, V. Bakken, C. Adamo, J. Jaramillo, R. Gomperts, R. E. Stratmann, O. Yazyev, A. J. Austin, R. Cammi, C. Pomelli, J. W. Ochterski, R. L. Martin, K. Morokuma, V. G. Zakrzewski, G. A. Voth, P. Salvador, J. J. Dannenberg, S. Dapprich, A. D. Daniels, Ö. Farkas, J. B. Foresman, J. V. Ortiz, J. Cioslowski and D. J. Fox, Gaussian 09, Revision A. 02 Gaussian, Inc., Wallingford, CT, USA, 2009.
15 L. Noodleman, *J. Am. Chem. Soc.*, 1981, **74**, 5737-5743.
16 P. Christian, G. Rajaraman, A. Harrison, M. Helliwell, J. J. W. McDouall, J. Raftery and R. E. P. Winpenny, *Dalton Trans.*, 2004, DOI: 10.1039/B407126C, 2550-2555.
17 E. Ruiz, J. Cano, S. Alvarez, A. Caneschi and D. Gatteschi, *J. Am. Chem. Soc.*, 2003, **125**, 6791-6794.
18 N. Berg, T. N. Hooper, J. Liu, C. C. Beedle, S. K. Singh, G. Rajaraman, S. Piligkos, S. Hill, E. K. Brechin and L. F. Jones, *Dalton Trans.*, 2013, **42**, 207-216.
19 G. Rajaraman, M. Murugesu, E. C. Sanudo, M. Soler, W. Wernsdorfer, M. Helliwell, C. Muryn, J. Raftery, S. J. Teat, G. Christou and E. K. Brechin, *J. Am. Chem. Soc.*, 2004, **126**, 15445-15457.
20 L. Fohlmeister, K. R. Vignesh, F. Winter, B. Moubaraki, G. Rajaraman, R. Pöttgen, K. S. Murray and C. Jones, *Dalton Trans.*, 2015, **44**, 1700-1708.
21 S. K. Singh, K. R. Vignesh, V. Archana and G. Rajaraman, *Dalton Trans.*, 2016, **45**, 8201-8214.
22 E. Cremades, J. Cano, E. Ruiz, G. Rajaraman, C. J. Milios and E. K. Brechin, *Inorg. Chem.*, 2009, **48**, 8012-8019.
23 K. R. Vignesh, S. K. Langley, K. S. Murray and G. Rajaraman, *Chem. Eur. J.*, 2015, **21**, 2881-2892.
24 F. Neese, *Wiley Interdisciplinary Reviews: Computational Molecular Science*, 2012, **2**, 73-78.